Surface plasmon interference formed by tightly focused higher polarization order axially symmetric polarized beams

Zhehai Zhou (周哲海)[1,2*], Qiaofeng Tan (谭峭峰)[1], and Guofan Jin (金国藩)[1]

[1]*State Key Laboratory of Precision Measurement Technology and Instruments, Tsinghua University, Beijing 100084, China*

[2]*Department of Optical Information Science and Technology, Beijing Information Science and Technology University, Beijing 100192, China*

[*]*E-mail: zhouzhehai@tsinghua.org.cn*

Received July 1, 2010

We numerically study the surface plasmon interference formed by tightly focused higher polarization order axially symmetric polarized beams (ASPBs) based on the vectorial diffraction theory. The definition of ASPBs is stated, and the optical setup for surface plasmon polariton (SPP) excitation and mathematical expressions for interfering SPP fields are proposed. The simulation results show that the interfering SPP fields present a multi-focal spot pattern. In addition, the number of spots is related to the polarization order of the incident beams P as $2\times(P-1)$, indicating potential utilization in near-field multiple optical trapping and near-field imaging and sensing. The unique interfering phenomenon is also explained.

OCIS codes: 240.0240, 110.0110, 260.0260.

doi: 10.3788/COL20100812.1178.

Interfering surface plasmon polaritons (SPPs) can be excited using a focused laser beam at normal incidence to a plane metal film, as first proposed by Kano *et al.*[1]. Other studies have also been conducted on the excitation of SPPs using linearly polarized beams[2], radially polarized beams[3−6], and even optical vortex beams[7−9]. These findings confirm the potential use of interfering SPPs in wide applications, such as in plasmonic devices, optical trapping, sensing, and near-field sub-diffraction imaging. In this letter, we extend the study of interfering SPPs formed by tightly focused higher polarization order axially symmetric polarized beams (ASPBs). We present the definition of ASPBs, propose a scheme to excite the interfering SPPs formed by tightly focused higher polarization order ASPBs, and derive the mathematical expressions of excited SPP fields near the metal surface using the vectorial diffraction theory. Numerical simulations are also used to demonstrate the unique SPP interference.

As mentioned in Refs. [10−13], ASPBs are space-variant, linearly polarized beams with axial symmetry. The symmetry axis is the propagation axis of the light beam. ASPBs are characterized by their polarization orientation. As shown in Fig. 1, the polarization orientation angle $\Phi(r,\phi)$ at an arbitrary point $S(r,\phi)$ only depends on the azimuthal angle ϕ as $\Phi(r,\phi)=P\times\phi+\phi_0$, where P is the polarization order and ϕ_0 is the initial polarization orientation when $\phi=0$. P equals the number of polarization rotations when ϕ gradually changes from 0 to 2π. A well-known form of cylindrical polarization is the axially symmetric polarization, with $P=1$. ASPBs can be generated by space-variant subwavelength dielectric gratings[14], liquid-crystal polarization converters[10], and other methods using a spatial light modulator (SLM)[15,16]. Previous researches[11−13] have shown that the focused fields of higher polarization order ASPBs present a multi-focal spot pattern, and that the size and number of spots are influenced by the polarization order of incident beams.

Figure 2(a) shows the model we analyze using the Kretschmann-Raether configuration. The configuration consists of a glass substrate, a metal thin film, and air. The ASPB is incident from the glass and focused on by a high numerical aperture (NA) objective lens (oil immersion). The beam is then focused on the interface between the glass substrate and the metallic film. When the ASPB converges toward the geometric focus, it gives rise to many diffraction-limited spots[10] that contain a large spectrum of in-plane wave vectors limited by the NA of the lens. At resonant angles $\pm\theta_{\rm sp}$, the wavevector-matched SPP waves can be generated, propagating radially at all azimuthal directions. These propagating SPP waves will interfere with one an-

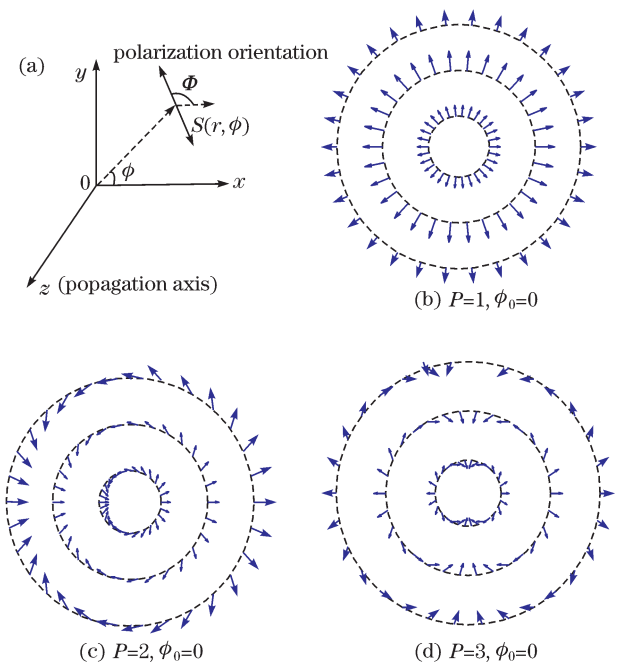

Fig. 1. (a) Polarization orientation of an ASPB, and (b)−(d) polarization distributions in the beam cross-section (x-y plane) for ASPBs with different polarization orders.

 © 2010 Chinese Optics Letters

other to form a standing wave, whose pattern is influenced by the amplitude and the phase of the incident beam.

The propagation constant of the SPP excited on the metal surface facing the air is approximately given by

$$k_{\mathrm{sp}}(\omega)=\frac{\omega}{c}\sqrt{\frac{\varepsilon_2(\omega)\,\varepsilon_3(\omega)}{\varepsilon_2(\omega)+\varepsilon_3(\omega)}}, \tag{1}$$

where ω denotes angular frequency, c denotes the light speed in vacuum, and $\varepsilon_2(\omega)$ and $\varepsilon_3(\omega)$ denote the relative permittivities of metal and air at the angular frequency of ω, respectively. The propagation constant of the light propagating in the glass substrate is

$$k_{\mathrm{incident}}=\frac{\omega}{c}\sqrt{\varepsilon_1(\omega)}\sin\theta_{\mathrm{sp}}, \tag{2}$$

where $\varepsilon_1(\omega)$ is the relative permittivity of the glass, and θ_{sp} is the surface plasmon resonance (SPR) angle. The resonance angle θ_{sp} strongly depends on the refractive index (or dielectric constant) profile of the sample within the evanescent field above the film surface. It is also usually larger than the total internal reflection critical angle. Resonant excitation occurs when the wavevector of the evanescent wave k_{incident} matches that of the SPP k_{sp}, which can be carried out using an oil-immersion objective lens with large NA.

Similar to Ref. [8], a 45-nm gold (Au) thin film with a complex permittivity of approximately −5.28+2.04i at the wavelength of 532 nm is considered for placement on a glass substrate. The theoretical SPR reflection curve with an angle modulation ranging from 30° to 80° is shown in Fig. 2(b), with a SPR angle of approximately 47.3°.

In a high-NA modeling system, the focal field of an ASPB is derived in Refs. [11−13] based on the full vectorial diffraction theory[17]. The field expression can be further simplified using Euler's formula,

$$\exp\{\mathrm{i}\,[(P-1)\,\phi+\phi_0]\}=\cos[(P-1)\,\phi+\phi_0]+\mathrm{i}\sin[(P-1)\,\phi+\phi_0], \tag{3}$$

and the following identities

$$\int_0^{2\pi}\exp[\mathrm{i}P\phi+\mathrm{i}kr_{\mathrm{s}}\sin\theta\cos(\phi-\phi_{\mathrm{s}})]\,\mathrm{d}\phi=2\pi\mathrm{i}^P\exp(\mathrm{i}P\phi_{\mathrm{s}})\,J_P(kr_{\mathrm{s}}\sin\theta), \tag{4a}$$

$$\int_0^{2\pi}\cos(\phi-\phi_{\mathrm{s}})\exp[\mathrm{i}P\phi+\mathrm{i}kr_{\mathrm{s}}\sin\theta\cos(\phi-\phi_{\mathrm{s}})]\,\mathrm{d}\phi=\pi\mathrm{i}^{P+1}\exp[\mathrm{i}P\phi_{\mathrm{s}}]\,[J_{P+1}(kr_{\mathrm{s}}\sin\theta)-J_{P-1}(kr_{\mathrm{s}}\sin\theta)]. \tag{4b}$$

Thus, the simplified focal field can be written as

$$\begin{bmatrix} E_r^{(\mathrm{s})}(r_{\mathrm{s}},\phi_{\mathrm{s}},z_{\mathrm{s}}) \\ E_\phi^{(\mathrm{s})}(r_{\mathrm{s}},\phi_{\mathrm{s}},z_{\mathrm{s}}) \\ E_z^{(\mathrm{s})}(r_{\mathrm{s}},\phi_{\mathrm{s}},z_{\mathrm{s}}) \end{bmatrix}=-\mathrm{i}^{(3P+1)}A\int_{\theta_{\min}}^{\theta_{\max}} l_0(\theta)\sqrt{\cos\theta}\sin\theta\exp(\mathrm{i}kz_{\mathrm{s}}\cos\theta)$$
$$\times\begin{bmatrix} \cos[(P-1)\phi_{\mathrm{s}}+\phi_0]\left\{\cos\theta\,[J_P(kr_{\mathrm{s}}\sin\theta)-J_{P-2}(kr_{\mathrm{s}}\sin\theta)]+J_P(kr_{\mathrm{s}}\sin\theta)+J_{P-2}(kr_{\mathrm{s}}\sin\theta)\right\} \\ \sin[(P-1)\phi_{\mathrm{s}}+\phi_0]\left\{\cos\theta\,[J_P(kr_{\mathrm{s}}\sin\theta)+J_{P-2}(kr_{\mathrm{s}}\sin\theta)]+J_P(kr_{\mathrm{s}}\sin\theta)-J_{P-2}(kr_{\mathrm{s}}\sin\theta)\right\} \\ 2\mathrm{i}\cos[(P-1)\phi_{\mathrm{S}}+\phi_0]\sin\theta J_{P-1}(kr_{\mathrm{S}}\sin\theta) \end{bmatrix}\mathrm{d}\theta. \tag{5}$$

Subsequently, the transmitted field on the film surface formed by tightly focused ASPBs, taking into account the multiple reflections for glass/Au/air configuration, can be further expressed as

$$\begin{bmatrix} E_r^{(\mathrm{s})}(r_{\mathrm{s}},\phi_{\mathrm{s}},z_{\mathrm{s}}) \\ E_z^{(\mathrm{s})}(r_{\mathrm{s}},\phi_{\mathrm{s}},z_{\mathrm{s}}) \end{bmatrix}=-\mathrm{i}^{(3P+1)}A\int_{\theta_{\min}}^{\theta_{\max}} l_0(\theta)\sqrt{\cos\theta}\sin\theta\exp\left[\mathrm{i}z_{\mathrm{s}}\sqrt{k_3^2-k_1^2\sin^2\theta}\right]t_{\mathrm{p}}(\theta)\cos[(P-1)\phi_{\mathrm{s}}+\phi_0]$$
$$\times\begin{bmatrix} \cos\theta\,[J_P(k_1r_{\mathrm{s}}\sin\theta)-J_{P-2}(k_1r_{\mathrm{s}}\sin\theta)]+J_P(k_1r_{\mathrm{s}}\sin\theta)-J_{P-2}(k_1r_{\mathrm{s}}\sin\theta) \\ 2\mathrm{i}\sin\theta J_{P-1}(k_1r_{\mathrm{s}}\sin\theta) \end{bmatrix}\mathrm{d}\theta. \tag{6}$$

where A is a constant; k_1, k_2, and k_3 are the wavelength numbers in the glass, Au film, and air, respectively; J_{P-2}, J_{P-1}, and J_P are the $(P-2)$th-order, $(P-1)$th-order, and Pth-order Bessel functions of the first kind, respectively; $\theta_{\min}$ and $\theta_{\max}$ are the minimum and maximum incident angles on the glass/Au interface corresponding to annular illumination, respectively; $l_0(\theta)$ is the pupil apodization function, which denotes the relative amplitude and phase of the incident ASPB; $t_{\mathrm{p}}(\theta)$ is the transmission coefficient of the p polarization of the three layers of configurations, which can be defined as

$$t_{\mathrm{p}}(\theta)=\frac{t_{12}^{\mathrm{p}}(\theta)\,t_{23}^{\mathrm{p}}(\theta)\exp\left(\mathrm{i}\sqrt{k_2^2-k_1^2\sin^2\theta}d\right)}{1+r_{12}^{\mathrm{p}}(\theta)\,r_{23}^{\mathrm{p}}(\theta)\exp\left(\mathrm{i}2\sqrt{k_2^2-k_1^2\sin^2\theta}d\right)}, \tag{7}$$

where d is the thickness of the Au thin film, t_{ij}^{p} and r_{ij}^{p}

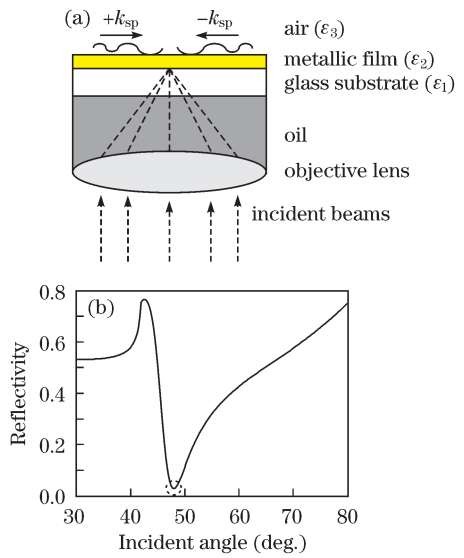

Fig. 2. (a) Kretschmann-Raether configuration for SPP excitation by means of an oil-immersion objective lens with high NA, and (b) theoretical SPR curve for Au configurations on conditions that ε_1=2.25 and ε_3=1.0.

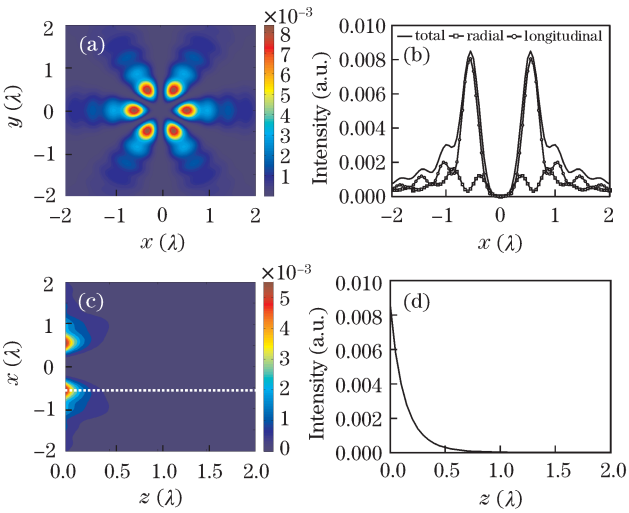

Fig. 3. Numerical simulation results for field intensity while the incident beam is a P=4 ASPB (ϕ_0=0°). (a) The total field intensity $|\mathbf{E}|^2$ on the film surface; (b) linescan of (a) along the x axis, the transverse component $|E_r|^2$, and longitudinal component $|E_z|^2$ are also shown; (c) total field intensity $|\mathbf{E}|^2$ along the optical axis near the film surface; (d) total field intensity $|\mathbf{E}|^2$ along the z axis.

are the transmission and reflection Fresnel coefficients of the p polarization of each of the two respective layer interfaces as shown in Fig. 2(a).

Based on the mathematical expressions shown in Eqs. (6) and (7), the numerical simulation of the field intensity $|\mathbf{E}|^2$ on the film surface is performed as shown in Fig. 3 while the incident beam is a P=4 ASPB, A=1.0, $\theta_{\min}$=45°, $\theta_{\max}$=49°. The pupil apodization function $l_0(\theta)$ is chosen as $l_0(\theta) = \exp\left[-\beta^2\left(\frac{\sin\theta}{\sin\theta_{\max}}\right)^2\right]\left(\sqrt{2}\beta\frac{\sin\theta}{\sin\theta_{\max}}\right)^P$, where β is the ratio of lens radius to beam width parameter at the lens, and β=1 is assumed here. The total field is the sum of the transverse component and the longitudinal component. Unlike those formed by other kinds of focused beams, the interfering SPP fields formed by higher polarization order ASPBs present a multi-focal spot pattern, and the number of spots is related with the polarization order P of the incident beams as $2\times(P-1)$. The intensity of the longitudinal component is larger than that of the radial component. Furthermore, the full-width of half-maximum (FWHM) of spots is nearly 0.34λ in the radial direction and 0.22λ in the longitudinal direction, which are both beyond the diffraction limit.

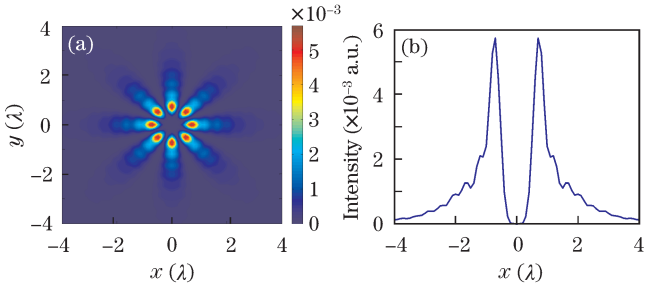

Fig. 4. Numerical simulation results for field intensity (P=5, ϕ_0=0°). (a) Total field intensity $|\mathbf{E}|^2$ on the film surface. (b) Linescan of (a) along the x axis.

Figure 4 shows another example corresponding to P=5 incident ASPB, further verifying our findings. The simulation results are similar to those shown in Fig. 3, but the number of spots is 8 and the size of the spots is almost unchanged.

We think the unique interfering phenomena are related with the unique polarization distributions of incident ASPBs. The polarization orientation variation of the incident beams with respect to the azimuthal angle results in the corresponding amplitude variation of p-polarized beams (along the radial direction). Only p-polarized beams can excite SPPs. Moreover, p-polarized beams with a periodic amplitude variation along the azimuthal direction will excite SPP waves with the corresponding amplitude variation, interfering with each other to form a multi-focal spot interfering pattern on the metal surface. The number of spots is the period of the SPP wave variation or $2\times(P-1)$.

In conclusion, we propose a scheme to excite interfering SPPs using tightly focused higher polarization order ASPBs. We demonstrate the optical setup and derive the mathematical expressions for interfering SPP fields. The simulation results show the unique field distribution with a multi-focal spot pattern, and indicate that the number and size of spots are related with the polarization order P of ASPBs, so we can manipulate the field distribution using different types of ASPBs. The unique interfering SPP fields with multiple ultrasmall focal spots on the film surface may be widely used in plasmonic devices, near-field multiple optical trapping, and sub-diffraction imaging and sensing.

This work was supported by the National "973" Program of China (No. 2007CB935303), the National Natural Science Foundation of China (No. 60908015), and the General Program of Beijing Municipal Commission of Education (No. KM200910772005).

References

1. H. Kano, S. Mizuguchi, and S. Kawata, J. Opt. Soc. Am. B **15,** 1381 (1998).
2. A. Bouhelier, F. Ignatovich, A. Bruyant, C. Huang, G. C. des Francs, J.-C. Weeber, A. Dereux, G. P. Wiederrecht, and L. Novotny, Opt. Lett. **32,** 2535 (2007).
3. Q. Zhan, Opt. Lett. **31,** 1726 (2006).
4. W. Chen and Q. Zhan, Proc. SPIE **6450,** 64500D (2007).
5. W. Chen and Q. Zhan, Opt. Lett. **34,** 722 (2009).
6. J. Yan, Y. Lu, P. Wang, C. Gu, R. Zheng, Y. Chen, H. Ming, and Q. Zhan, Chin. Opt. Lett. **7,** 909 (2009).
7. P. S. Tan, X.-C. Yuan, J. Lin, Q. Wang, T. Mei, R. E. Burge, and G. G. Mu, Appl. Phys. Lett. **92,** 111108 (2008).
8. P. S. Tan, X.-C. Yuan, J. Lin, Q. Wang, and R. E. Burge, Opt. Express **16,** 18451 (2008).
9. Z. J. Hu, P. S. Tan, S. W. Zhu, and X.-C. Yuan, Opt. Express **18,** 10864 (2010).
10. M. Stalder and M. Schadt, Opt. Lett. **21,** 1948 (1996).
11. Z. Zhou, Q. Tan, and G. Jin, Chin. Opt. Lett. **7,** 938 (2009).
12. L. Li, Chin. Opt. Lett. **8,** 1110 (2010).
13. Z. Zhou, Chin. Opt. Lett. **8,** 1112 (2010).
14. A. Niv, G. Biener, V. Kleiner, and E. Hasman, Opt. Lett. **28,** 510 (2003).
15. J. A. Davis, D. E. McNamara, D. M. Cottrell, and T. Sonehara, Appl. Opt. **39,** 1549 (2000).
16. X. Wang, J. Ding, W. Ni, C. Guo, and H. Wang, Opt. Lett. **32,** 3549 (2007).
17. Q. Zhan, Adv. Opt. Photon. **1,** 1 (2009).